9950-1035

DRL No. 216
DRD No. SE-3

DOE/JPL 956831-3
Distribution Category UC-63

# ARCO Solar, Inc.

## Quarterly Report No. 3

## PULSED EXCIMER LASER PROCESSING FOR COST-EFFECTIVE SOLAR CELLS

**JPL Contract No. 956831**

**Reporting Period: November 1984 - January 1985**



Prepared for

California Institute of Technology
Jet Propulsion Laboratory
4800 Oak Grove Drive
Pasadena, California 91109

Submitted by

ARCO Solar, Inc.
P. O. Box 2105
Chatsworth, California 91313

DRL No. 216
DRD No. SE-3

DOE/JPL 956831-3
Distribution Category UC-63

# PULSED EXCIMER LASER PROCESSING FOR COST-EFFECTIVE SOLAR CELLS

Quarterly Report No. 3

November 1984 - January 1985


Prepared By

D. Wong
Principal Investigator

Approved By

W. R. Dottenberg
Program Manager

ARCO Solar, Inc.
P. O. Box 2105
Chatsworth, California 91313



The JPL Flat-Plate Solar Array Project is sponsored by the U.S. Department of Energy and forms part of the solar Photovoltaic Conversion Program to initiate a major effort toward the development of low-cost solar arrays. This work was performed for the Jet Propulsion Laboratory, California Institute of Technology, by agreement between NASA and DOE.

This work was performed for the Jet Propulsion Laboratory, California Institute of Technology, and was sponsored by the U.S. Department of Energy through an agreement with the Naticnal Aeronautics and Space Administration.

**ABSTRACT**

Residual lattice damage by 5 keV ion implantation as well as surface flaws induced by wafer cleaning have been proven to affect the $V_{OC}$ more adversely for laser-annealed cells than conventional thermal-diffusion. However, an alternative, molecular implantation of molecular species holds potential. The first experimental results are encouraging, although further investigation and tests would be required. The lack of a commercially available mass-analyzed implantation with low energy, high fluence ions is constraining.

**CONTENTS**

**CONTENTS**
**(Continued)**

Tables

**CONTENTS**
**(Continued)**

Figures

## SECTION 1.0
## INTRODUCTION AND SUMMARY

It has been shown that most standard 5 keV ion implantation processes create significant detrimental impact on the open circuit voltage ($V_{OC}$) of laser annealed cells. A detailed and systematic investigation of all previous data on 3" diameter FZ wafers has led to the hypothesis that one cause of voltage loss is lattice damage due to residual high energy neutral dopant atoms in the ion beam. In a 5 keV ion implantation process, the dopant ions are accelerated to 35 keV. Some ions are neutralized at the wall while still traveling at high kinetic energy and these atoms are unaffected by the 30 keV reversal field. Lattice damage by such high energy particles in a "low energy" implantation would be at a depth beyond the annealing range of 1.5 J/cm$^2$ laser energy density.

$V_{OC}$ was also shown to be impaired by the effects of standard surface cleaning processes used to minimize the optical and recrystallization impact of surface flaws. The results of various experiments suggest that the surface should be cleaned by a high pressure water jet to remove surface contaminants and spin-dried in a controlled atmosphere to avoid the formation of water spots.

p+nn+ cells were processed during this period. Ion implantation was performed at 5 keV with a non-mass analyzed molecular ion beam for the front and 15 keV for a back surface field (BSF). Data analysis shows the potential of such cells to reach the goal of over 16% efficiency by improving ion implant conditions and contact resistance. Such molecular beam ion implantation is considered promising for phosphorus implants into p-type substrates. The kinetic energy of the atomic phosphorus unit may be decreased to as low as 3 keV, at least by theoretical calculation.

## SECTION 2.0
## EXPERIMENTAL PROGRESS

### 2.1 ION IMPLANTATION ALTERNATIVES

The six 1"x1" samples of Cz silicon wafers sent to the University of Illinois Coordinated Science Laboratory for implantation with As at 500 eV using a low energy ion gun have not yet been returned. Arsenic has been chosen in this trial because no changes in the setup are required.

The glow discharge ion implantation concept has been put aside.

### 2.2 LASER-ASSISTED CVD EQUIPMENT

The gas distribution system and deposition chamber for laser-assisted chemical vapor deposition of metal grids and passivating layers has been assembled and checked out. The system includes a Matheson Gas Products three gas cabinet, gas flow metering hardware, mixing manifold, pump/purge system, gas reaction chamber, sample heater, control panel and gas scrubber. The system will be shipped in March to Spectra Tecnology where the experimental work will take place. Spectra Technology personnel who will use the system assisted in final checkout and have been trained in the safe operating procedures and safety features of the system.

### 2.3 LASER EQUIPMENT

Variations in laser pulse duration and energy density were investigated during this quarter to obtain the best junction dopant profiles possible using commercially available ion implant sources. The best pulse duration found was 25 nsec and the optimum laser energy density was 1.5 J/cm$^2$. The 25 nsec pulse duration is the same as that used in Batch 26, which has yielded the highest efficiency solar cells (15.8% with AR coating). A long laser pulse duration (40 nsec) results in a junction depth that is too deep to obtain high solar cell efficiency. Laser energy density was varied between 1.35 J/cm$^2$ and 1.6 J/cm$^2$; the higher values caused surface damage and the lower values did not fully anneal the junction.

The method of focusing the output of the beam homogenizer onto the wafer was modified by using two lenses instead of one, thereby providing sharper focus and a more uniform laser beam spatial intensity profile (see Quarterly Report No. 2 for details of analysis).

Laser diagnostics were installed and used to record the laser output energy during the equivalent of a complete scan of a 4" diameter wafer (27,000 pulses). No dropouts occurred; the laser

energy was found to be within a band that is ±5% of the average.

The laboratory layout for the metallization process step was established and the design for the optical assembly completed. Mechanical components are being fabricated. Optical components coated for 193 nm were ordered, including a cylindrically focusing lens, unstable resonator cavity mirrors and windows for the laser, and turning mirrors for the optical beam positioning assembly. Most of the optical mounts, as well as the x-y motor-driven translation stages and controls, are already available.

### 2.3.1 Laser Pulse Waveform Modification

The laser pulse waveform used earlier (Quarterly Report No. 2, Figs. 2-11a and 2-11b) showed two peaks with a significant dip in intensity between the peaks. The electrical drive circuit produced forward current (first laser peak) followed by current reversal (second laser peak). The circuit was modified by reducing the peaking capacitance at the laser head from 12 nF to 3 nF, and connecting a 4 nF pulse forming line to the laser head. This circuit eliminated current reversal and led to the pulse waveform shown in Fig. 2-11c of Quarterly Report No. 2. The pulse duration for this case is 35 nsec.

A further change in the laser circuit was made by introducing a transformer in the preionizer network. This produced an earlier preionization discharge that could be timed relative to the main discharge voltage rise to achieve optimum discharge stability and laser output stability. The resulting pulse waveform, used for Batch 35, is shown in Fig. 2-1a. The effective pulse duration is 40 nsec. Wafers annealed using this longer pulse duration were found to yield low efficiency solar cells due to the junction being too deep.

The electrical drive circuit was modified further to reduce the pulse duration to that previously in Batch 26. The 4 nF capacitance was reduced to 3.5 nF, and the inductance was reduced, yielding the waveform shown in Fig. 2-1b (25 nsec pulse duration).

### 2.3.2 Optics Modifications

Previous analysis of the focusing optics used to image the output of the beam homogenizer onto the wafer had shown that the edges of the beam were not as sharply defined as they could be (Quarterly Report No. 2). Furthermore, previous experiments had shown that better solar cell results were obtained if the laser spot was sharply focused on the wafer than if it was defocused. For these reasons, the single lens focusing arrangement was modified by adding a second lens. The spacing between the lenses, the distance from the beam homogenizer, and the distance to the wafer all can be varied individually by micrometer-driven

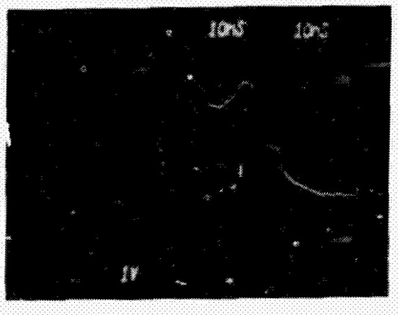

a. 40 nsec pulse duration (Batch 35)

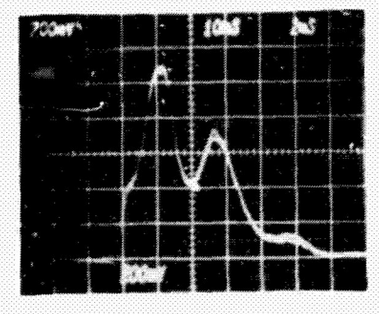

b. 25 nsec pulse duration (Batch 37)

**Fig. 2-1.** Laser pulse waveforms with modified driver and preionizer circuits.

slides. The lens added has a focal length of 40 mm and a diameter of 25 mm.

The resulting laser spot using two lenses was found to be considerably more uniform, based on measuring the spot size dimension on photosensitive paper as a function of beam attenuation using neutral density filters. The intensity falloff at the edge occurs over a dimension of 0.05 mm for a spot size of 1.0 mm.

### 2.3.3 Laser Diagnostics

During this quarter the digital photodiode developed previously was used to monitor the individual laser pulse energy as a function of repetition rate. Fig. 2-2 shows some of the results obtained using this probe. Energy increases ~5% as the laser warms up. This change appears to plateau after about 1000 pulses. The same behavior was observed at 10 Hz rep rate. The short-term energy fluctuations appear smaller at 20 Hz than at 10 Hz (not shown). When wafers are processed, the laser is operated at 20 Hz for 2 minutes to reach steady output before the beam is directed on the wafer.

The raster scanning software was modified during the past month to allow real-time monitoring of the output energy during a scan. The modified software allows continuous storage of the energy data to diskette, at the end of each row, so that complete energy data for an entire processed wafer may be analyzed later. Up to 65,000 shots can be stored in this fashion.

Figs. 2-3 and 2-4 show results obtained with the photodiode probe. The periodicity in the patterns corresponds to turning on the laser at the beginning of each row. The first pulse in each series in Fig. 2-3 appears to be consistently high. Since the scan begins slightly off the wafer surface, this effect is not expected to be a problem.

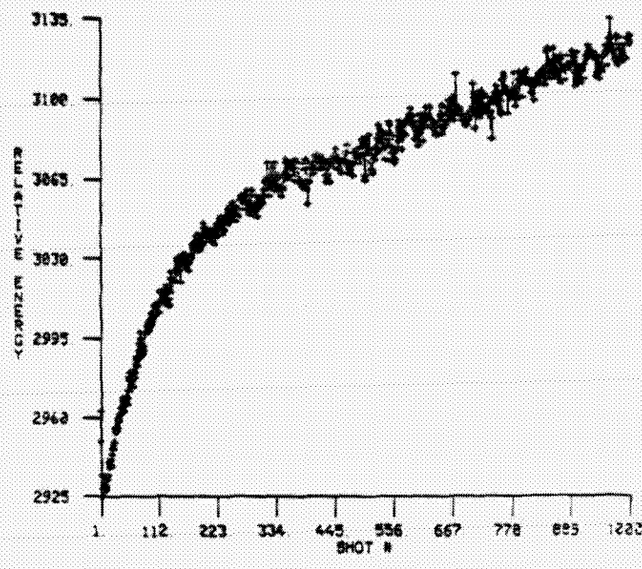


**Fig. 2-2.** Laser energy vs. shot number for 1000 shots at 20 Hz repetition rate.

The magnitude of each laser pulse was monitored during actual processing of wafers (Fig. 2-4). The detector was placed to view the weak 308 nm output transmitted through the high reflectivity cavity mirror of the laser. It was found that the signal was slightly modulated by the motion of the wafer table due to feedback of visible fluorescence from the glass wafer holder induced by each laser output pulse The fluorescence retraces the optical train to the laser and is readily transmitted through the UV-coated laser cavity mirrors to the detector. The fluorescence signal was absent when the laser beam impinged on the wafer rather than on the glass plate because the wafer does not fluorescence significantly.

For the results shown in Fig. 2-4, the motorized table is programmed for a 4.2"-long scan pattern in steps of 0.020", beginning just off a 4" diameter wafer. Each row of spots is spaced 0.021". Each cross in the figure represents a laser pulse. The low initial signal level is background noise due to the room lights before the laser is activated. During the early portion of the record, the laser spot is near the edge of the wafer and the detector signal corresponds to the laser spot hitting the glass plate most of the time. Later in the record the scan of the laser spot is near the middle of the wafer and the detector signal corresponds to the spot hitting the wafer most of the time. The first 7000 pulses of the run are shown here. The complete wafer required 27,000 pulses.

In the complete scan of the wafer there were no laser pulse dropouts. The modulation of the detector signal was 10% of the basic signal, and the variability of the laser energy remained within $\pm$5% for the complete scan of the wafer.

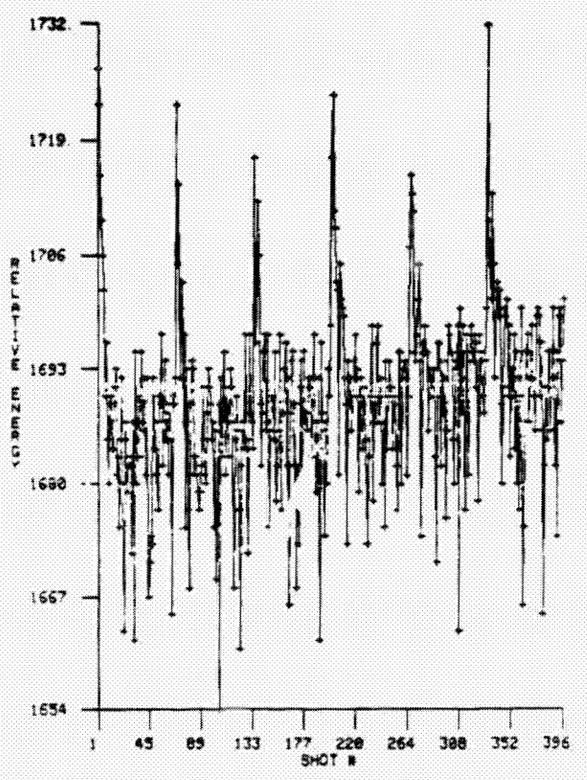


**Fig. 2-3.** Laser pulse output vs. shot number taken during an actual raster scan.

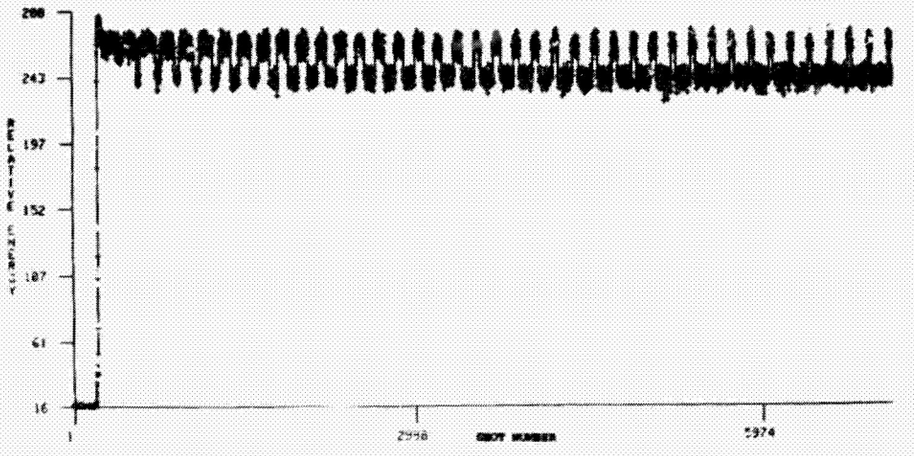


**Fig. 2-4.** Monitor of laser pulse energy during laser annealing of 4" diameter wafer. Regular modulation of the detector signal is due to reflections, not to laser energy variations.

### 2.3.4 Laser Annealing of Wafers

Several types of ion-implanted wafers were laser annealed during this quarter. The conditions for these processing experiments are listed in Table 2-1. However, not all annealed wafers were processed into cells since most of the experiments were for the purpose of surface studies.

### 2.3.5 Metallization and Passivation Process Steps

The design of the optical system was completed during this quarter; laser modifications needed for studies of photochemical vapor deposition for the passivation and metallization process steps also were completed. The objective cylinder lens to be used to form a line focus for the metallization process step was analyzed using the three-dimensional, extended source, ray trace code. Two commercially available lenses were studied. The first was a plano-cylinder lens with a nominal paraxial focal length of 100 mm. This lens produces a minimum blur square 90 microns in size at a working distance of 83.5 mm. The second lens was a best form lens also with a nominal focal length of 100 mm. This lens produces a blur square size of 40 microns at a working distance of 72 mm. Both lenses were studied assuming an input beam from an extended source of 1.2x1.2 cm with a 0.1 mrad half angle beam divergence. These parameters are expected of the laser using unstable resonator optics. Thus it appears that the inherent laser and lens performance will meet the metallization line width requirements when used at this f number of six. The superior performance of the best form lens indicates that this lens should be purchased.

Also during this reporting period, the specification of unstable resonator optics for the laser at 193 nm was completed and a suitable vendor for the optics and coatings was located. The cavity will consist of a 200 cm radius of curvature plano-convex high reflector and a 75 cm meniscus output coupler with a dot high reflection coating of 3.75 mm diameter. The latter will be AR-coated for 193 nm on the second surface, and the two optics will be separated by 62.5 cm, providing for a cavity magnification of ~2.7. Both substrates are made of suprasil quartz and are stock items.

The optical assembly for the metallization process step is shown in Figs. 2-5 and 2-6. The laboratory layout is similar to that shown in Quarterly Report No. 1. The laser beam is reflected off a 45-degree turning mirror and directed to the metallization processing optical assembly. The beam enters parallel to the axis of motion of the upper motorized translation stage, then is deflected 90 degrees, making it parallel to the axis of motion of the lower translation stage. The beam is then reflected downward through a cylindrically focusing lens and through the UV

Table 2-1. Laser annealing parameters.

| Batch | Laser Energy (mJ) | Spot Size (mmxmm) | Average Energy Density ($J/cm^2$) | Table Speed (cm/sec) | Spot Interval (mmxmm) |
|---|---|---|---|---|---|
| **Pulse duration = 40 nsec; overlap = 50%** | | | | | |
| Batch 35: 3" 5 keV p-type FZ | | | | | |
| 1 wafer | 13 | 0.9x0.9 | 1.6 | 0.9 | 0.45x0.45 |
| Batch 35: 4"x4" thermal diffusion p-type Cz | | | | | |
| 2 wafers | 13 | 0.9x0.9 | 1.6 | 0.9 | 0.45x0.45 |
| Batch 36: 3" 5 keV p-type FZ | | | | | |
| 1 wafer | 12 | 0.95x0.95 | 1.33 | 0.9 | 0.45x0.45 |
| **Pulse duration = 25 nsec; overlap = 50%** | | | | | |
| Batch 37: 3" 5 keV p-type FZ (modified PFN) | | | | | |
| 2 wafers | 14 | 1.0x1.0 | 1.4 | 1.0 | 0.5x0.5 |
| Batch 38: 3" 5 keV p-type FZ (modified focus optics) | | | | | |
| 2 wafers | 14.5 | 1.0x1.05 | 1.4 | 1.0 | 0.5x0.55 |
| Batch 38: 2"x2" 5 keV p-type Cz | | | | | |
| 2 wafers | 13.5 | 1.0x1.05 | 1.3 | 1.0 | 0.5x0.55 |
| Batch 39: 3" 5 keV p-type FZ (no surface change due to laser) | | | | | |
| 2 wafers | 14 | 1.0x1.0 | 1.4 | 1.0 | 0.5x0.5 |
| 1 wafer | 13 | 1.0x1.0 | 1.3 | 1.0 | 0.5x0.5 |
| Batch 40: 4"x4" n-type Cz | | | | | |
| 1 wafer | | | | | |
| 5 keV front | 14.5 | 1.0x1.05 | 1.4 | 1.0 | 0.5x0.55 |
| 35 keV back | 14 | 0.75x0.75 | 2.5 | 0.8 | 0.4x0.4 |
| Batch 40: 3" n-type Cz | | | | | |
| 1 wafer | | | | | |
| spin-on source on back | 14 | 0.75x0.75 | 2.5 | 0.8 | 0.4x0.4 |

**Table 2-1.** Laser annealing parameters (continued).

| Batch | Laser Energy (mJ) | Spot Size (mmxmm) | Average Energy Density ($J/cm^2$) | Table Speed (cm/sec) | Spot Interval (mmxmm) |
|---|---|---|---|---|---|
| **Pulse duration = 25 nsec; overlap = 50%** | | | | | |
| Batch 41: 3" 5 keV n-type Cz | | | | | |
| 2 wafers front | 14 | 0.95x1.0 | 1.45 | 1.0 | 0.47x0.5 |
| 1 wafer spin-on back | 14 | 0.75x0.8 | 2.3 | 0.8 | 0.38x0.4 |
| 2 wafers repeat back* | 14 | 0.60x0.65 | 3.5 | 0.6 | 0.25x0.25 |
| Batch 42: 2"x2" 5 keV p-type Cz | | | | | |
| 2 quadrants | 13.5 | 0.95x0.95 | 1.5 | 1.2 | 0.38x0.38 |
| Batch 43: 2"x2" 5 keV p-type Cz | | | | | |
| 5 wafers | 14 | 0.90x1.0 | 1.5 | 0.9 | 0.36x0.40 |
| Batch 44: 2"x2" 5 keV p-type Cz | | | | | |
| 2 wafers | 14 | 0.92x1.0 | 1.5 | 0.9 | 0.36x0.4 |
| Batch 45: 2"x2" 5 keV p-type Cz | | | | | |
| 1 wafer | 14.5 | 0.92x1.0 | 1.5 | 0.9 | 0.36x0.4 |
| 1 wafer | 14.5 | 1.00x1.05 | 1.4 | 1.0 | 0.4x0.42 |
| Batch 46: 4"x4" 5 keV p-type Cz (Zymet ion implant) | | | | | |
| 1 wafer | 14.5 | 1.00x1.05 | 1.4 | 1.0 | 0.4x0.42 |

*Annealed twice with overlap = 60%.

transparent window of the metallization process chamber. The wafer is located in a fixed position inside the chamber. The optics are adjusted to provide best focus of the laser beam at the plane of the wafer and proper orientation of the line focus relative to the direction of motion of the motorized translation stages.

The 45-degree turning mirrors are 2" in diameter, large enough to accomodate the full laser beam. The cylinder lens is mounted on an x-y-z translation stage to center the lens with the center of the laser beam, and to adjust the focal plane relative to the wafer. The lens is mounted in a rotary stage to align the line focus with the direction of travel of one or the other of the motorized translation stages. In this way long metallization

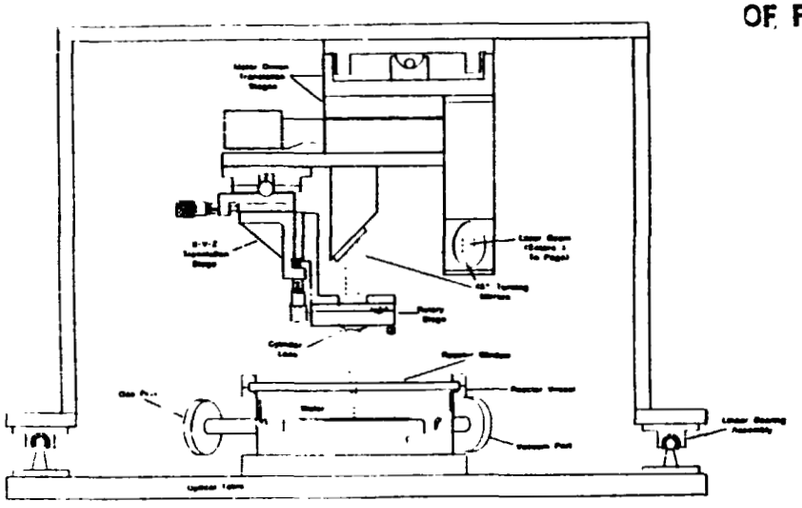

**Fig. 2-5.** Scale drawing of optical assembly for metallization process step.

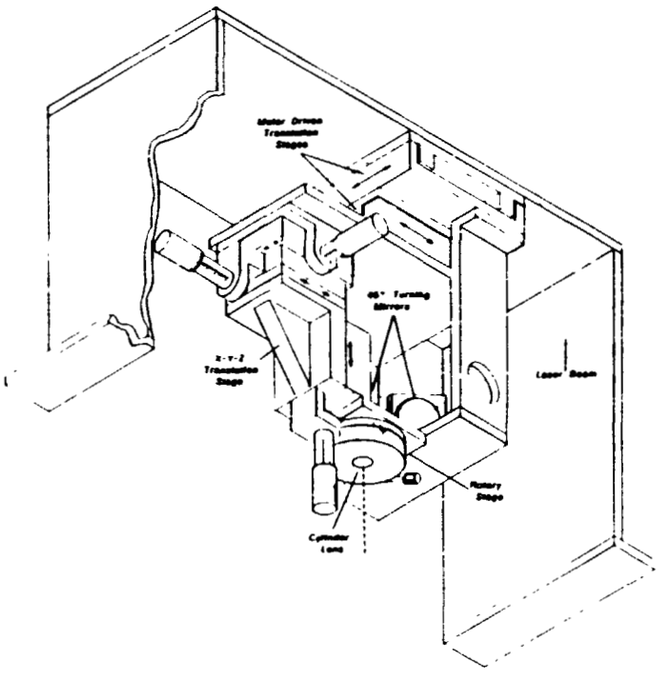

**Fig. 2-6.** Isometric view of optical assembly showing motion of translation stages.

lines can be made of line segments laid down end to end on the wafer. The line segments will be 1-2 cm long using this optical arrangement. The widths of the line will be 50-100 microns, using unstable resonator optics on the laser.

The whole optical assembly will be mounted on rigid rails and rolled aside to permit access to the gas chamber in order to change wafers. With the optics moved to one side, the top flange holding the UV window will be unbolted and removed, permitting the previous wafer to be removed and a new wafer installed.

Detailed design of the optical assembly has been completed and the mechanical parts are being fabricated. Assembly will begin early in March.

Many of the optic holders and motorized translation stages to be used are already available from the build-up of the laser annealing assembly. The common components of the two processes will not be duplicated because of cost. The changeover from the metallization process to the laser annealing process will be made as rapidly and as conveniently as possible; however, a period of several hours will be required for rearrangement and realignment of the optical assemblies each time there is a change from one process to the other.

## 2.4 LASER ANNEALING EXPERIMENT

### 2.4.1 Surface Condition

#### 2.4.1.1 Cleaning Procedure

As reported in Quarterly Reports No. 1 and No. 2, surface conditions affect the $V_{OC}$ and fill factor of laser annealed cells more seriously than conventional thermal diffused cells. It was also reported that the chemical etching-cleaning did not thoroughly remove particulates. Such particulates can become nucleation centers upon laser annealing at melting temperature. Light scrubbing with cloth and detergent was found capable of reducing, but not totally removing, the surface contamination. However, such a cleansing procedure has been found to be detrimental to the ion implanted surface.

Samples of 3" diameter FZ p-type wafers with 5 keV $^{31}P^{+}$ ion implant were divided into lots to test for the effects of different surface preparation techniques (Fig. 2-7).

The in-house chemical cleaning included $H_2SO_4$ + $H_2O_2$ at elevated temperature followed by 10% HF + 15% HCl etching and rinsing before scrubbing with detergent. The light and hard scrubbing were defined respectively as with and without pressure during scrubbing. Wafers were examined under microscope after laser annealing at 1.3 J/cm$^2$ or 1.4 J/cm$^2$ (Fig. 2-8). Results suggest

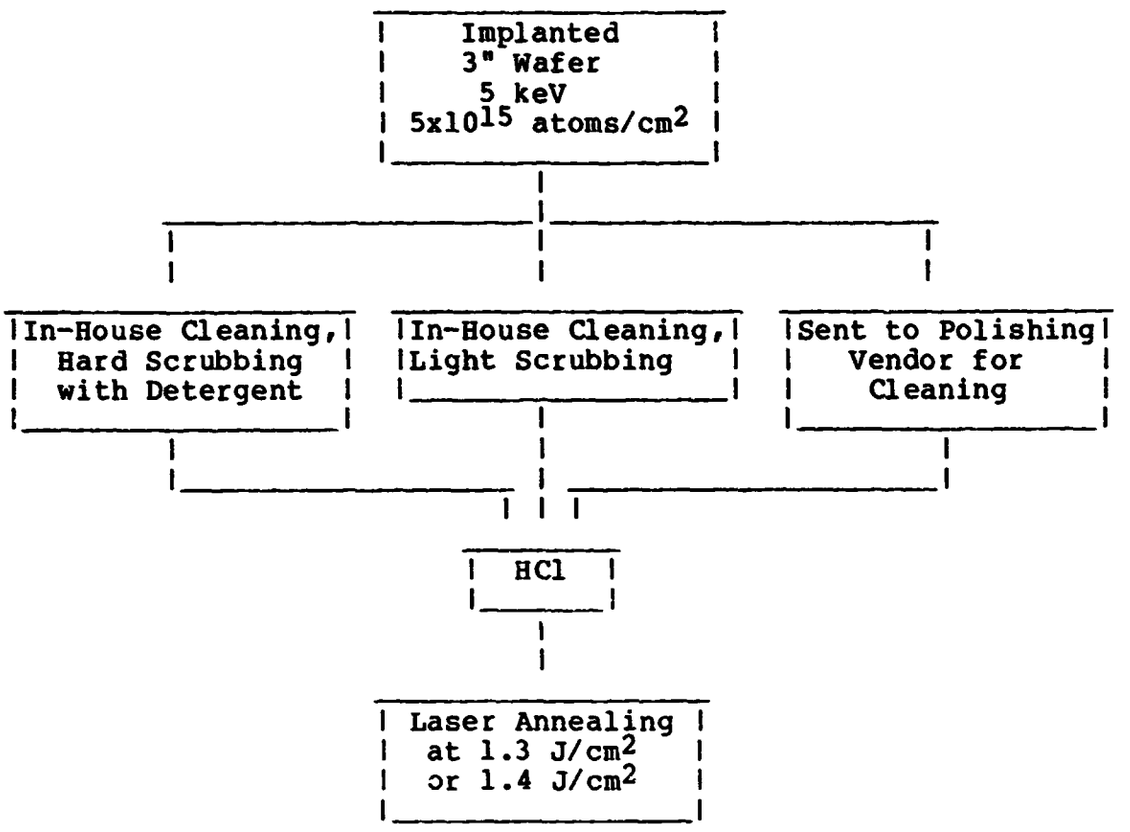


**Fig. 2-7.** Comparison of surface preparation techniques.

that hard scrubbing damaged the surface by introducing microscratches. However, hard scrubbing on wafers without ion implant did not show scratches after laser annealing, indicating the difference in hardness between the ion implanted layer and the crystalline silicon surface.

Surface damage on wafers cleaned by the vendor was even more severe (Fig. 2-9). Scratches were of the linear type. Microdefects ("haze"), on the other hand, were found to be of lower density than found with scrubbing.

The results suggest, in general, that mechanical scrubbing causes surface damage on ion implanted wafers. However, surface damage defects were not observable prior to laser annealing. Apparently laser annealing of silicon surfaces may be used to reveal surface defects, as an alternative to using preferential etchants such as Sirtl and Seecco.

Hard scrubbing on ion implanted wafers apparently almost removes the implant layer. The sheet rho of wafers cleaned with hard scrubbing often exceeded 200 ohms/square.

a. Light scrubbing; 1.3 J/cm$^2$

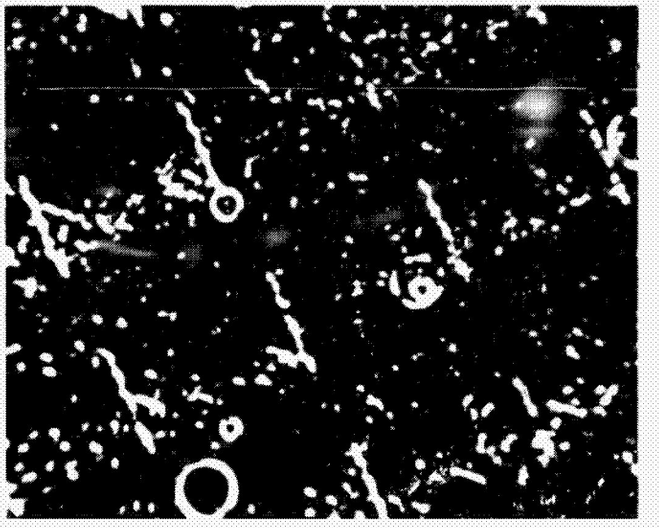

b. Hard scrubbing; 1.3 J/cm$^2$

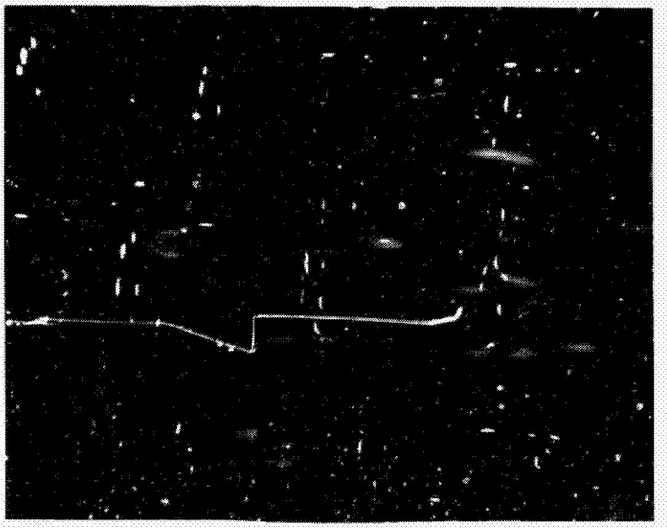

c. Light scrubbing; 1.4 J/cm$^2$

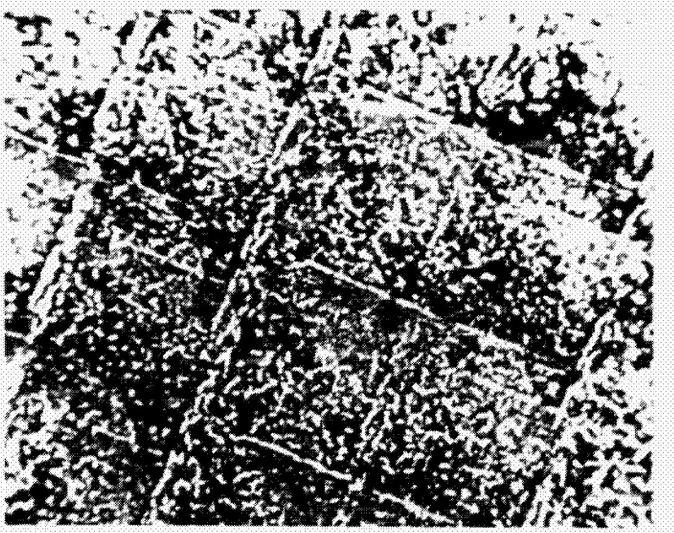

d. Hard scrubbing; 1.4 J/cm$^2$

**Fig. 2-8.** Wafers cleaned in-house and then laser annealed.

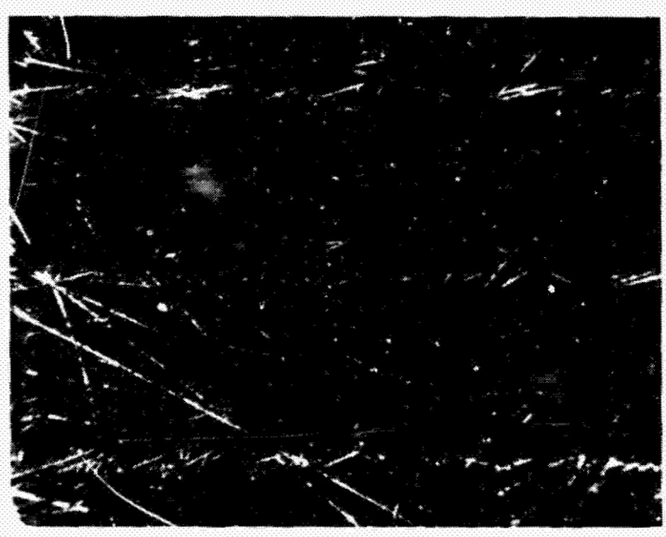

**Fig. 2-9.** Wafer cleaned by vendor after ion implant.

### 2.4.1.2 Effects of DI Water

As the laser project has progressed, the effects of surface conditions and surface contamination on laser annealed cells have become better understood. The DI water system was redesigned to upgrade its quality. As a result, the water resistance is as high as 18 megohms with 5 micron absolute filtration. Water of such high resistance is usually considered to be excellent DI water quality. However, analysis of accumulated data led to the discovery that water resistance is only one of the basic requirements. The other important factor is the presence of sub-micron particulates that are apparently non-polarizable and thus not conductive enough to be detected by the resistance probes. Such particulates may cause serious reduction in fill factor of laser annealed cells.

A clear example occurred during the cleaning of wafers before laser annealing, where the water resistance was observed to decrease from 16 megohms to 13 megohms. Water transparency was then tested by shining a coherent light through it. A column of haze was seen, indicating that the light was being scattered by fine particles. Installation of a 0.2 micron filter greatly reduced the haze. The 0.2 micron filter later was found to be completely blocked after 3 hours of water flow. Visual examination of the filter element revealed a slightly brownish film. The exact nature of the particulates is not known; chemical analysis is under way.

The cells made from the experiments, with and without the use of a 0.2 micron filter, were electrically characterized (Table 2-2). Also included were control cells that were thermally diffused and metallized simultaneously.

Table 2-2. Wafers cleaned without and with 0.2 micron filter. DI water resistance ~16-13 megohms. Wafers ion implanted at 5 keV, $3x10^{15}$ atoms/cm$^2$; laser energy 1.5 J/cm$^2$, 50% overlap.

a. Wafers cleaned without 0.2 micron filter.

| Sample No. | $J_{sc}$ mA/cm$^2$ | $V_{oc}$ (V) | FF (%) | Eff (%) |
|---|---|---|---|---|
| B44-1.5 | | | | |
| #1 | 20.05 | 0.580 | 61.66 | 7.17 |
| #2 | 20.43 | 0.580 | 70.75 | 8.40 |
| #3 | 18.19 | 0.582 | 64.35 | 6.82 |
| #4 | 17.20 | 0.575 | 58.57 | 5.79 |
| Control R59I | | | | |
| #1 | 21.92 | 0.595 | 77.54 | 10.11 |
| #2 | 22.15 | 0.596 | 77.65 | 10.25 |

b. Wafers cleaned with 0.2 micron filter.

| Sample No. | $J_{sc}$ mA/cm$^2$ | $V_{oc}$ (V) | FF (%) | Eff (%) |
|---|---|---|---|---|
| B45-1.5 | | | | |
| #1 | 19.39 | 0.583 | 77.54 | 8.76 |
| #2 | 20.26 | 0.583 | 76.24 | 9.01 |
| #3 | 20.20 | 0.583 | 76.84 | 9.05 |
| #4 | 19.89 | 0.583 | 77.54 | 8.99 |
| Control B45 R59II | | | | |
| #1 | 21.36 | 0.589 | 78.09 | 9.82 |
| #2 | 21.89 | 0.591 | 77.83 | 10.07 |

As the data show, the main difference between these two groups of cells is in the fill factor, which is much poorer in cells cleaned without a 0.2 micron filter.

### 2.4.2 Junction Formation: p-Type Substrates

For the quarter, major effort was devoted to repeating the experiment (B26) that yielded the 15.9% (AR-coated) cell reported in Quarterly Report No. 2. However, none of the attempts has been successful. Besides the surface conditions mentioned above, it is felt that the laser energy density problems and ion implantation problems are two of the handicaps that limited reproducibility.

### 2.4.2.1 Laser Energy Density

Two experiments (B38 and B45) were performed to test for the difference between higher and lower energy density annealing on two different kinds of substrates, FZ and Cz. Cell performance is summarized in Table 2-3.

**Table 2-3.** Comparison of higher and lower energy density annealing on Cz and FZ material.

a. FZ material ion implanted at 5 keV, $5 \times 10^{15}$ atoms/cm$^2$. Base resistivity ~0.3 ohm-cm.

| Sample No. | $J_{sc}$ mA/cm$^2$ | $V_{oc}$ (V) | FF (%) | Eff (%) |
|---|---|---|---|---|
| B38 -- energy density = 1.3 J/cm$^2$ | | | | |
| #1 | 21.03 | 0.585 | 61.35 | 7.55 |
| #2 | 20.42 | 0.591 | 77.22 | 9.32 |
| B38 -- energy density = 1.4 J/cm$^2$ | | | | |
| #1 | 20.18 | 0.590 | 73.52 | 8.75 |
| #2 | 20.51 | 0.593 | 74.61 | 9.08 |
| #3 | 19.40 | 0.593 | 76.25 | 8.77 |

b. Cz material ion implanted at 5 keV, $3 \times 10^{15}$ atoms/cm$^2$. Base resistivity ~1 ohm-cm.

| Sample No. | $J_{sc}$ mA/cm$^2$ | $V_{oc}$ (V) | FF (%) | Eff (%) |
|---|---|---|---|---|
| B45 -- energy density = 1.4 J/cm$^2$ | | | | |
| #1 | 18.82 | 0.576 | 76.8 | 8.33 |
| #2 | 20.46 | 0.568 | 69.1 | 8.03 |
| #3 | 20.21 | 0.577 | 74.3 | 8.66 |
| #4 | 20.51 | 0.578 | 72.2 | 8.56 |
| B45 -- energy density = 1.5 J/cm$^2$ | | | | |
| #1 | 19.39 | 0.583 | 77.54 | 8.76 |
| #2 | 20.26 | 0.583 | 76.24 | 9.01 |
| #3 | 20.20 | 0.583 | 76.84 | 9.05 |
| #4 | 19.89 | 0.583 | 77.54 | 8.99 |

The results indicate a trend of higher fill factor and $V_{oc}$ when higher laser energy (varied from 1.3 J/cm$^2$ to 1.5 J/cm$^2$) is used. A junction depth profile of sample B45-1.4 J/cm$^2$ shows a slight "kink" at 0.18 micron, which clearly suggests incomplete

annealing; no such curve shape change appears on the B45-1.5 J/cm$^2$ sample (Fig. 2-10). Severe surface damage begins at energy density $\geq$1.6 J/cm$^2$. From this it is concluded that a narrow process window exists for energy density from 1.4 to 1.6 J/cm$^2$.

### 2.4.2.2 Ion Implant Conditions

**Effects of Damage by 5 keV Ion Implant.** Two key experiments (Batch 35 and Batch 36) were performed early in the quarter to investigate performance effects from lattice damage caused by 5 keV ion implantation. These represent extensions on the Batch 15 experiment, reported in Quarterly Report No. 1, in that thermal n+ deposition was used instead of ion implant. A thermal deposition of dopant source represents a zero lattice damage case in comparison to any ion implant source. Lower laser annealing energy densities and smaller overlaps than in Batch 15 were also employed.

In Batch 35, laser energies of 1.6 J/cm$^2$ with 50% overlap were used. The four comparison process sequences are shown in Fig. 2-11. Average performances of the four groups of cells (made from a 3" FZ wafer for ion implant Case A, and a 4" Cz wafer for thermal deposition Cases B, C, and D) are given in Table 2-4.

The low sheet rho for Case C (laser annealed cells with phosphorus glass) is consistent with results from Batch 15 in that the phosphorus glass layer acted as a high concentration doping source. Spreading resistance measurements on these cells (Fig. 2-12) suggest that the various junction depths correlate well with the differences in $J_{sc}$ among these cells and that shallow junctions give rise to higher current collections.

The results of the $V_{oc}$ measurements, however, are rather interesting. Case C (Cz, n+ thermal deposition followed by laser annealing) has the highest $V_{oc}$, about 8 mV higher than Case A (FZ, low bulk resistivity, ion implanted, laser annealed). The difference in $V_{oc}$ between the two is believed to be due to residual lattice damage by ion implantation.

The second experiment, Batch 36, used the same ion implanted FZ material as Batch 35 except that the laser annealing energy was reduced to 1.33 J/cm$^2$. Control cells to monitor wafer cleaning and metallization were thermally diffused Cz cells. Results show that both the $V_{oc}$ and fill factor of ion implanted cells decrease in comparison with Batch 35, while the control cells behaved typically for 1 ohm-cm Cz material without BSF (Table 2-5). These results indicate that reducing the annealing energy increases the amount of non-removable lattice damage induced by 5 keV ion implantation.

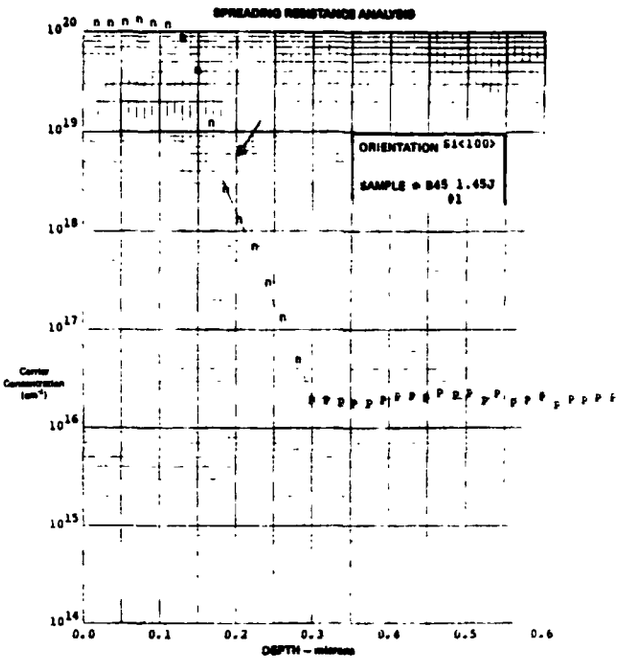


a. B45-1.4 J/cm$^2$ annealed at 1.4 J/cm$^2$, 50% overlap.

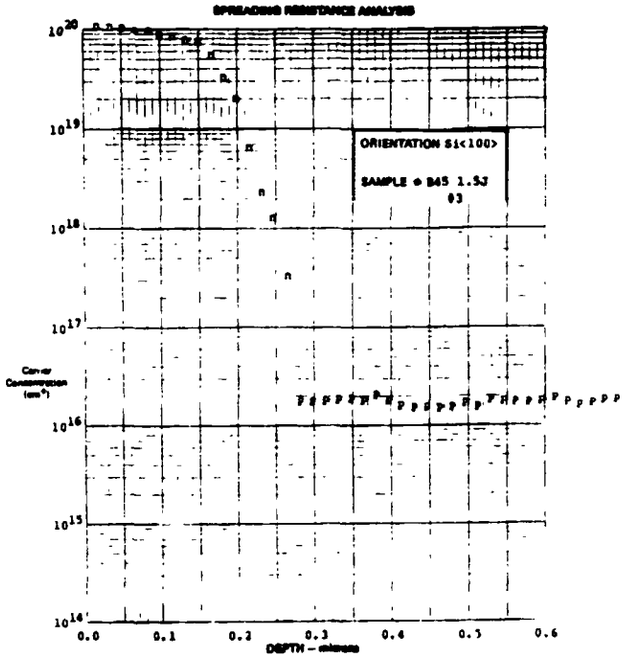


b. B45-1.5 J/cm$^2$ annealed at 1.5 J/cm$^2$, 50% overlap.

**Fig. 2-10.** Depth profiles of Batch 45 cells.

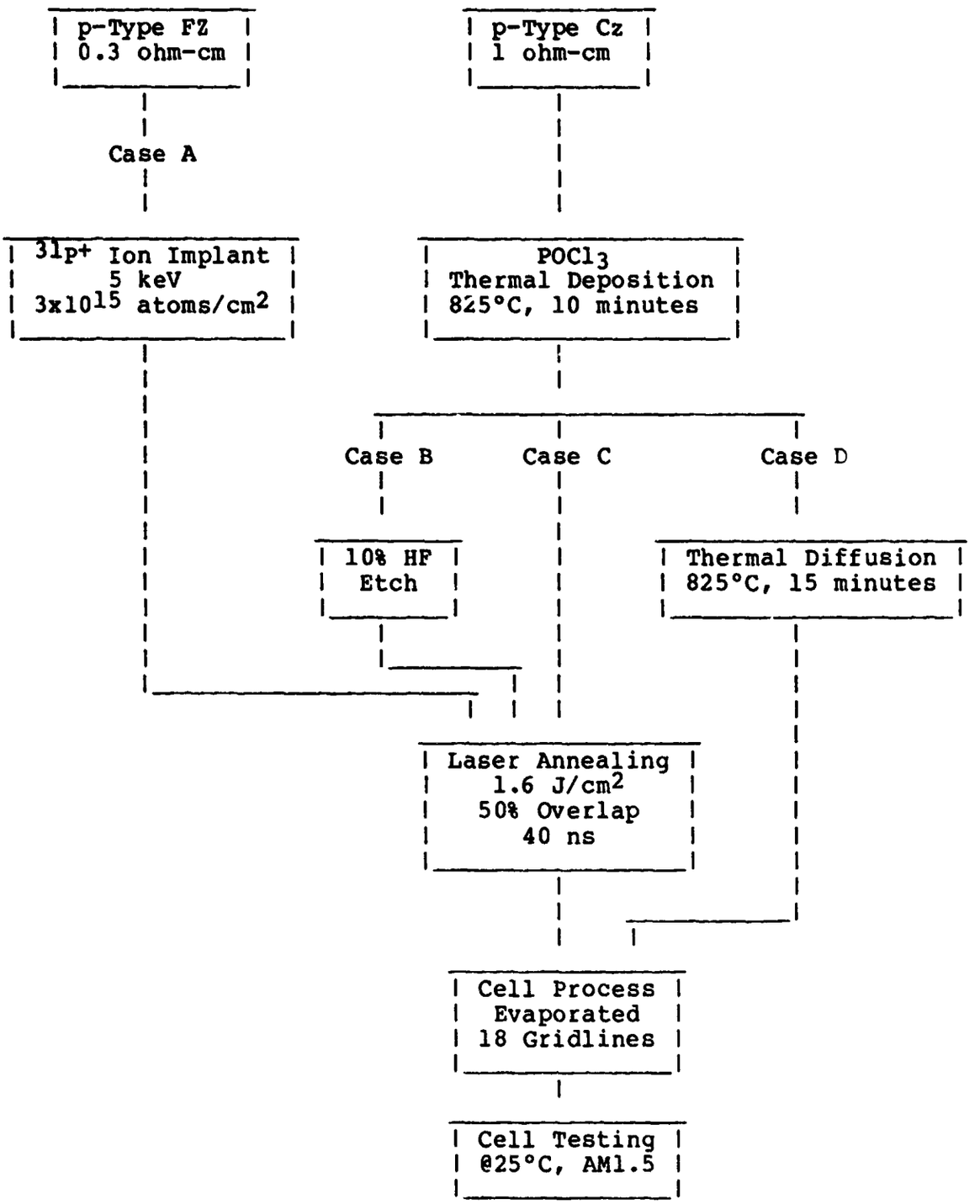


**Fig. 2-11.** Process sequence for Batch 35.

**Table 2-4.** Average performance of Batch 35 cells. Laser energy density at 1.6 J/cm$^2$, 50% overlap with 40 ns pulse duration.

| Sample | $J_{sc}$ (mA/cm$^2$) | $V_{oc}$ (V) | FF (%) | Eff (%) | Sheet Rho (ohm/sq) | Junction Depth (micron) |
|---|---|---|---|---|---|---|
| Case A FZ, 0.3 ohm-cm, 5 keV, 31P+ ion implant 3x10$^{15}$ atoms/cm$^2$ | 21.02 | 0.588 | 75.10 | 9.28 | 85 | 0.35 |
| Case B Cz, 1 ohm-cm, thermal $POCl_3$ deposition + HF + laser annealing | 19.20 | 0.587 | 73.80 | 8.3 | 65 | 0.45 |
| Case C Cz, 1 ohm-cm, thermal $POCl_3$ deposition + laser annealing | 19.80 | 0.596 | 75.44 | 8.9 | 23 | 0.49 |
| Case D Cz, 1 ohm-cm, thermal $POCl_3$ deposition + thermal diffusion | 21.38 | 0.590 | 74.24 | 9.3 | 140-150 | 0.27 |

**Effects of "Neutrals" on Mass Analyzed Ion Implantation.** The best cell obtained so far in the project has been from Batch 26, in which $^{31}P^+$ ion was implanted onto 2"x2" Cz material at 5 keV with fluence 2.5x10$^{15}$ atoms/cm$^2$. The ion implanted material was used through experiments B24, B26, and B28. In all three experiments, the average cell efficiency was above 9.5%, which was comparable to thermally diffused Cz cells. At the same time, the 5 keV, 5x10$^{15}$ atoms/cm$^2$ ion implanted 3" (diameter) FZ material was about 8.5-9% in efficiency overall. Discussion with the implant vendor indicated that the Cz material was implanted with the presence of "neutral" traps while the FZ was not. The "neutrals" came from ionized phosphorus atoms accelerated to 35 keV which were electrically neutralized at the walls before reaching the decelerating field. Such neutrals would continue to travel with 35 keV impact kinetic energy unaffected by the reversing 30 kV potential. The penetration depth by such high energy atoms would be more than 0.4 micron. This is a potential explanation for poorer fill factor.

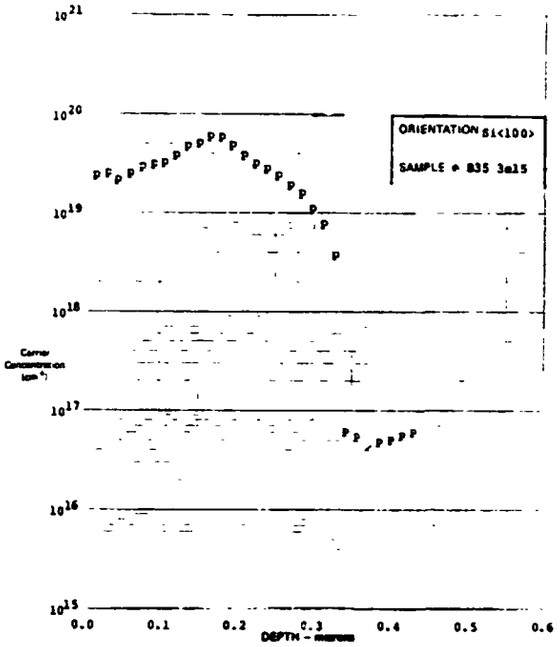


Case A. FZ; ion implant
+ laser anneal

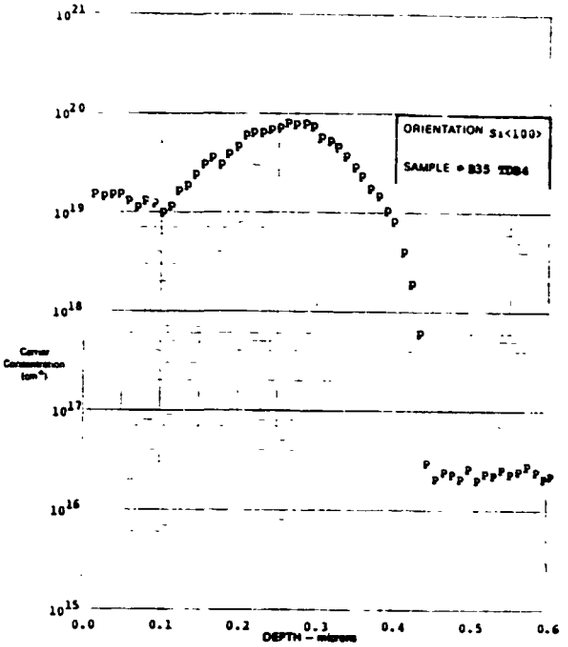


Case B. Cz; thermal deposition
+ HF + laser anneal

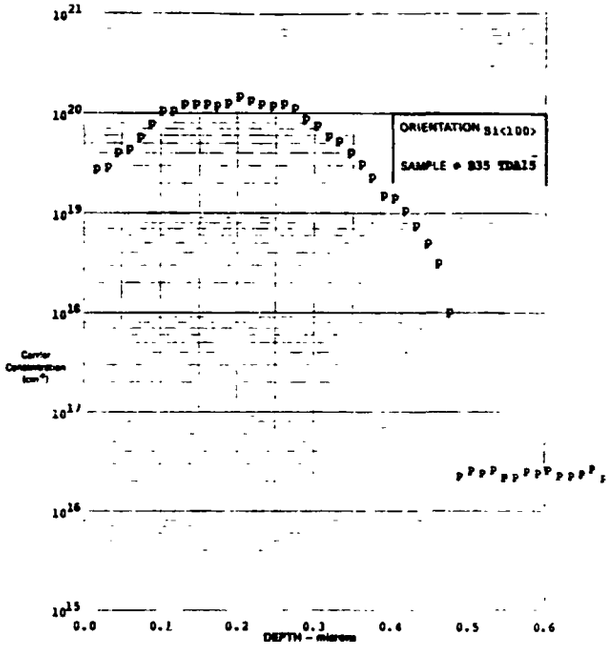


Case C. Cz; thermal deposition
+ laser anneal

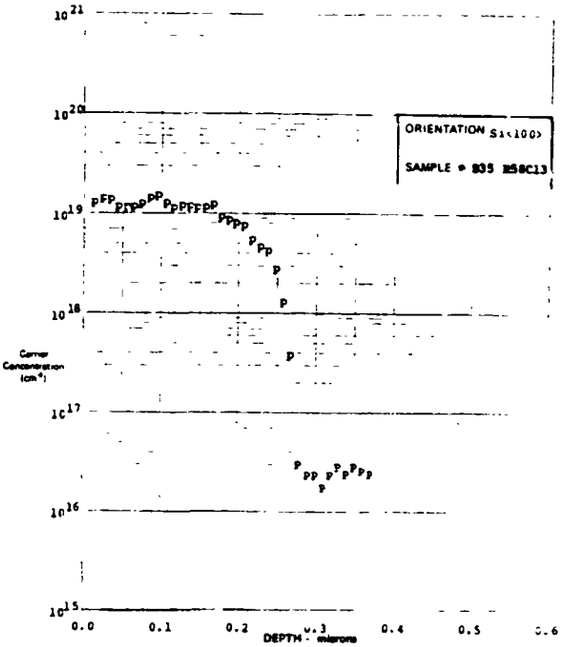


Case D. Cz; thermal deposition
+ thermal diffusion

**Fig. 2-12.** Depth profiles of Batch 35 cells.

**Table 2-5.** Performance of Batch 36 annealed at 1.33 J/cm$^2$, 50% overlap with pulse duration of 40 nsec (no AR coating).

| Sample No. | $J_{sc}$ (mA/cm$^2$) | $V_{oc}$ (V) | FF (%) | Eff (%) | Sheet Rho (ohm/sq) |
|---|---|---|---|---|---|
| FZ; 0.3 ohm-cm; ion implant B363E15 | | | | | |
| #1 | 20.96 | 0.580 | 74.17 | 9.02 | ~100 |
| #2 | 21.02 | 0.573 | 72.80 | 8.77 | " |
| #3 | 21.25 | 0.580 | 76.09 | 9.38 | " |
| #4 | 20.78 | 0.576 | 67.60 | 8.10 | " |
| #5 | 20.71 | 0.572 | 64.45 | 7.64 | " |
| #6 | 20.97 | 0.576 | 73.40 | 8.86 | " |
| Average | 20.95 | 0.576 | 71.42 | 8.60 | ~100 |
| Cz; 1 ohm-cm; thermal diffusion R59CI | | | | | |
| #1 | 21.42 | 0.597 | 78.28 | 10.01 | ~90 |
| #2 | 21.51 | 0.596 | 79.91 | 10.24 | " |
| #3 | 21.60 | 0.596 | 78.82 | 10.15 | " |
| #4 | 21.35 | 0.595 | 79.42 | 10.09 | " |
| Average | 21.47 | 0.596 | 79.11 | 10.12 | ~90 |

More 2"x2" Cz material was submitted for ion implant with neutral trap conditions specified. Cells fabricated from these batches (B44, B45) again were disappointing. The poor result from B44 was obviously due to the water conditions (see discussion above). The B45 experiment, however, used good DI water with a 0.2 micron filter. Here the poor results may be related to the ion implant conditions (annealed at 1.5 J/cm$^2$; see Table 2-1). The vendor's records show that the wafers were implanted without target rotation, giving rise to poor sheet rho uniformity. Four-point measurements on annealed wafers indicate a large variation (20 ohms/sq) in surface resistance from the center toward the edge of the wafer.

To test for the quality of the ion implanted n+ layer, a wafer from this group was then thermally annealed at 850°C for 30 minutes followed by 1.5 hours at 550°C low temperature annealing. Only two cells survived the process. The results from this and from the thermally diffused cells are presented in Table 2-6. Also included for comparison are the results from the laser annealed wafers B45-1.5J (also reported above in Table 2-3).

**Table 2-6.** Comparison of thermally annealed and laser annealed wafers.

| Sample No. | $J_{sc}$ (mA/cm$^2$) | $V_{oc}$ (V) | FF (%) | Eff (%) | Sheet Rho (ohm/sq) |
|---|---|---|---|---|---|
| B45 -- ion implant; thermally annealed | | | | | |
| #1 | 18.84 | 0.579 | 72.67 | 7.92 | 35 |
| #2 | 19.24 | 0.575 | 73.05 | 8.08 | " |
| B45 -- 1.5 J/cm$^2$; laser annealed | | | | | |
| #1 | 19.39 | 0.583 | 77.54 | 8.76 | 35-45 |
| #2 | 20.26 | 0.583 | 76.24 | 9.01 | " |
| #3 | 20.20 | 0.583 | 76.84 | 9.05 | " |
| #4 | 19.89 | 0.583 | 77.54 | 8.99 | " |
| Control -- R59; thermal diffusion | | | | | |
| #1 | 21.36 | 0.589 | 78.09 | 9.82 | 100 |
| #2 | 21.69 | 0.591 | 77.83 | 10.07 | " |

The data from both laser and thermally annealed cells are similar. In fact, the former has slightly higher value in current, $V_{oc}$, and fill factor. These experiments show three crucial points: Low energy ion implant requires the use of neutral traps; laser processed cells can be made equivalent to thermally processed cells; and water quality for surface preparation processes is very important before laser processing steps.

Optical micrographs taken at 800x on such a laser annealed sample revealed for the first time the microdefects (Fig. 2-13) at a high surface density. While no exact explanation to their origin has yet been determined, surface contaminants could be one of the sources. The structures also look like segregation cells formed during the recrystallization from the melt of an initial ion dose of $2.5 \times 10^{15}$ atoms/cm$^2$ (see A.G. Cullis et al., 1981), except the size is almost 100 times too large. One thing is certain: such structures are related to ion implantation and laser annealing, as indicated by Fig. 2-14. There are no microdefects in regions that were not ion implanted. Samples have been submitted for SIMS analysis.

The presence of microdefects affects the $V_{oc}$ substantially. All recently laser annealed samples from this implanted group have such defects on the surface, although the density varies from sample to sample and depends on laser energy density.

**Non-Mass Analyzed Molecular Ion Implantation.** Besides using the conventional mass-separated atomic ion implantation for emitter formation, a molecular ion implant process was also attempted. The vendor subjected samples of 4" square, 1 ohm-cm p-type Cz material to $PF_3^+$ ion implantation at the calculated 3 keV energy

**Fig. 2-13.** Microdefects on B45 cell after laser annealing at 1.5 J/cm$^2$, 50% overlap. $^{31}P^+$ ion implanted at 5 keV, $2x10^{15}$/cm$^2$. 800x magnification.

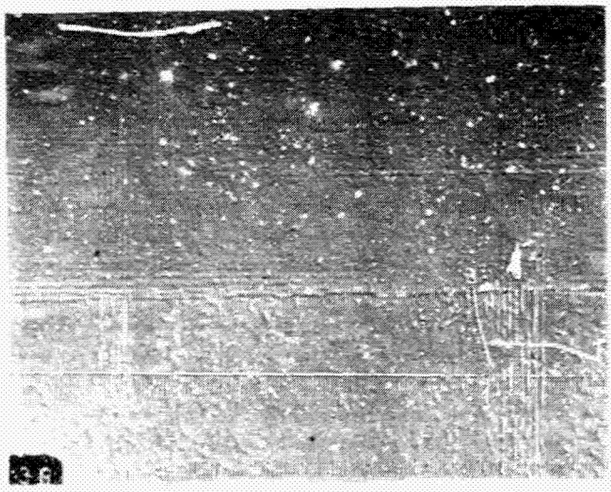


**Fig. 2-14.** Differences in surface structure between ion implanted and non-implanted areas after 1.5 J/cm$^2$, 50% overlap laser annealing. 200x magnification.

with fluence $3x10^{15}$ atoms/cm$^2$. After cleaning, wafers were annealed at energy 1.4 J/cm$^2$, 50% overlap. Sheet rho was about 110 ohms/sq, which is high for an actual $3x10^{15}$ atomic implant. It is possible that a large portion of the molecular ion bounced off the surface instead of penetrating into the substrate. Cells were tested as usual (Table 2-7). The majority of the cells are above 9% in efficiency with three at or above 9.4%, a substantially better performance than previous experiments.

**Table 2-7.** Cz p-type material subjected to molecular ion implant.

| Sample No. | $J_{sc}$ (mA/cm$^2$) | $V_{oc}$ (V) | FF (%) | Eff (%) |
|---|---|---|---|---|
| B46 | | | | |
| #1 | 20.66 | 0.574 | 72.30 | 8.58 |
| #2 | 21.13 | 0.579 | 77.48 | 9.48 |
| #3 | 20.16 | 0.575 | 75.78 | 8.79 |
| #4 | 20.17 | 0.577 | 76.30 | 8.87 |
| #5 | 20.50 | 0.577 | 76.00 | 9.00 |
| #6 | 20.87 | 0.578 | 78.2 | 9.44 |
| #7 | 20.74 | 0.577 | 75.74 | 9.07 |
| #8 | 20.97 | 0.58 | 80.00 | 9.71 |
| Average | 20.65 | 0.577 | 76.48 | 9.11 |

### 2.4.3 Junction Formation: n-Type Substrates

Batch 40 ion-implanted n-type substrates were 4" diameter Cz (4-6 ohm-cm) material 12 mils thick with one side chemically and mechanically polished (chem-mech polished or CMP). The implant was performed using non-mass analyzed molecular ions of mainly $BF_2^+$ at a calculated 5 keV energy of fluence $3.5x10^{15}$ atoms/cm$^2$ on the emitter side, and $PF_3$ at 15 keV on the back for the BSF. Laser process energy density on the front (emitter) was 1.4 J/cm$^2$and on the back was 2.5 J/cm$^2$. The sheet resistivity after annealing was 38-40 ohm/sq (front) and 11 ohm/sq (back).

Electrical measurements of these cells (Table 2-8) show low $V_{oc}$, suggesting the BSF was not effective. The surprisingly low $J_{sc}$ for high bulk resistivity material (4 ohm-cm) was probably due to poor bulk material, recombination in the diffused layer, and/or high contact resistance. Spectral response measurement of these n-type cells, however, show much higher quantum efficiency at long wavelengths but poor efficiency in the blue compared with the thermally diffused cells (Fig. 2-15). $J_{sc}$ calculated by integrating the spectral response data suggests a value of 23 mA/cm$^2$ instead of 21 mA/cm$^2$ as measured by light I-V (Fig. 2-16).

**Table 2-8.** Performance of Batch 40 p+nn+ Cz cells. Base resistivity ~4-6 ohm-cm. BSF ion-implanted n+ with phosphorus at 15 keV, $1x10^{16}$ atoms/$cm^2$ followed by laser annealing at 1.5 J/$cm^2$, 50% overlap.

| Sample No. | $J_{sc}$ (mA/$cm^2$) | $V_{oc}$ (V) | FF (%) | Eff (%) | Sheet Rho (ohm/sq) |
|---|---|---|---|---|---|
| B40 (p+nn+) | | | | | |
| # 1 | 21.41 | 0.546 | 75.51 | 8.83 | 38-40 |
| # 2 | 20.97 | 0.551 | 76.04 | 8.78 | " |
| # 3 | 21.07 | 0.550 | 76.17 | 8.83 | " |
| # 4 | 21.28 | 0.550 | 75.38 | 8.83 | " |
| # 5 | 20.98 | 0.553 | 76.01 | 8.82 | " |
| # 6 | 20.83 | 0.547 | 75.15 | 8.57 | " |
| # 7 | 21.84 | 0.549 | 75.37 | 9.04 | " |
| # 8 | 21.96 | 0.550 | 75.62 | 9.13 | " |
| # 9 | 21.30 | 0.545 | 74.92 | 8.69 | " |
| #10 | 22.00 | 0.539 | 74.72 | 8.86 | " |
| #11 | 21.39 | 0.532 | 72.82 | 8.29 | " |
| #12 | 21.55 | 0.544 | 75.27 | 8.81 | " |
| Average | 21.38 | 0.546 | 75.24 | 8.78 | 38-40 |
| Control Cell (Cz n+p) | | | | | |
| R59II #1 | 21.54 | 0.593 | 78.34 | 10.00 | 100 |
| R59I #2 | 22.22 | 0.597 | 79.48 | 10.55 | " |

Together with the dark I-V curve data (Fig. 2-16), it is concluded that these p+nn+ cells have relatively high series resistance that limits the $J_{sc}$. In fact, junction depth profiling (Fig. 2-17) shows a rather sharp and shallow junction characteristic which favors higher current collection. However, a hump appears at a depth of about 0.15 micron, suggesting incomplete laser annealing as well as the existence of an electrically "dead" layer. The former affects the $V_{oc}$ and the latter causes poor short wavelength response. This hypothesis agrees well with the spectral response and light I-V measurements discussed above.

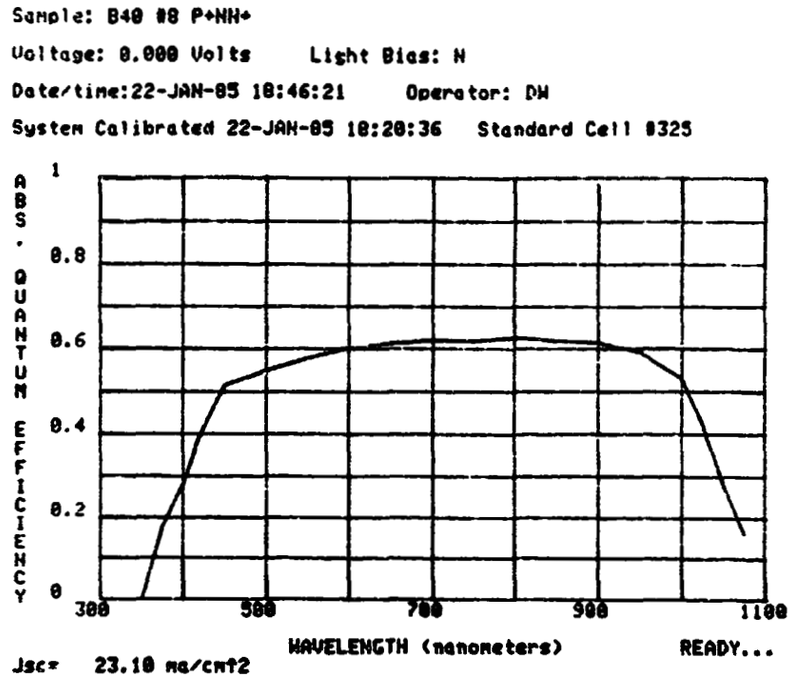


Spectral response of n-type Cz cell.

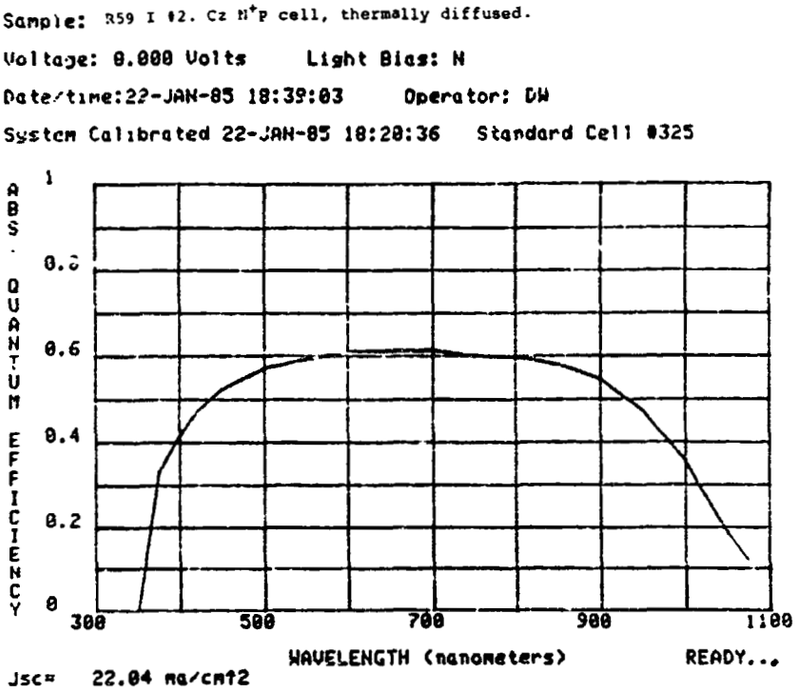


Spectral response of control cell from thermally diffused Cz wafer.

**Fig. 2-15.** Spectral response of Batch 40 cells.

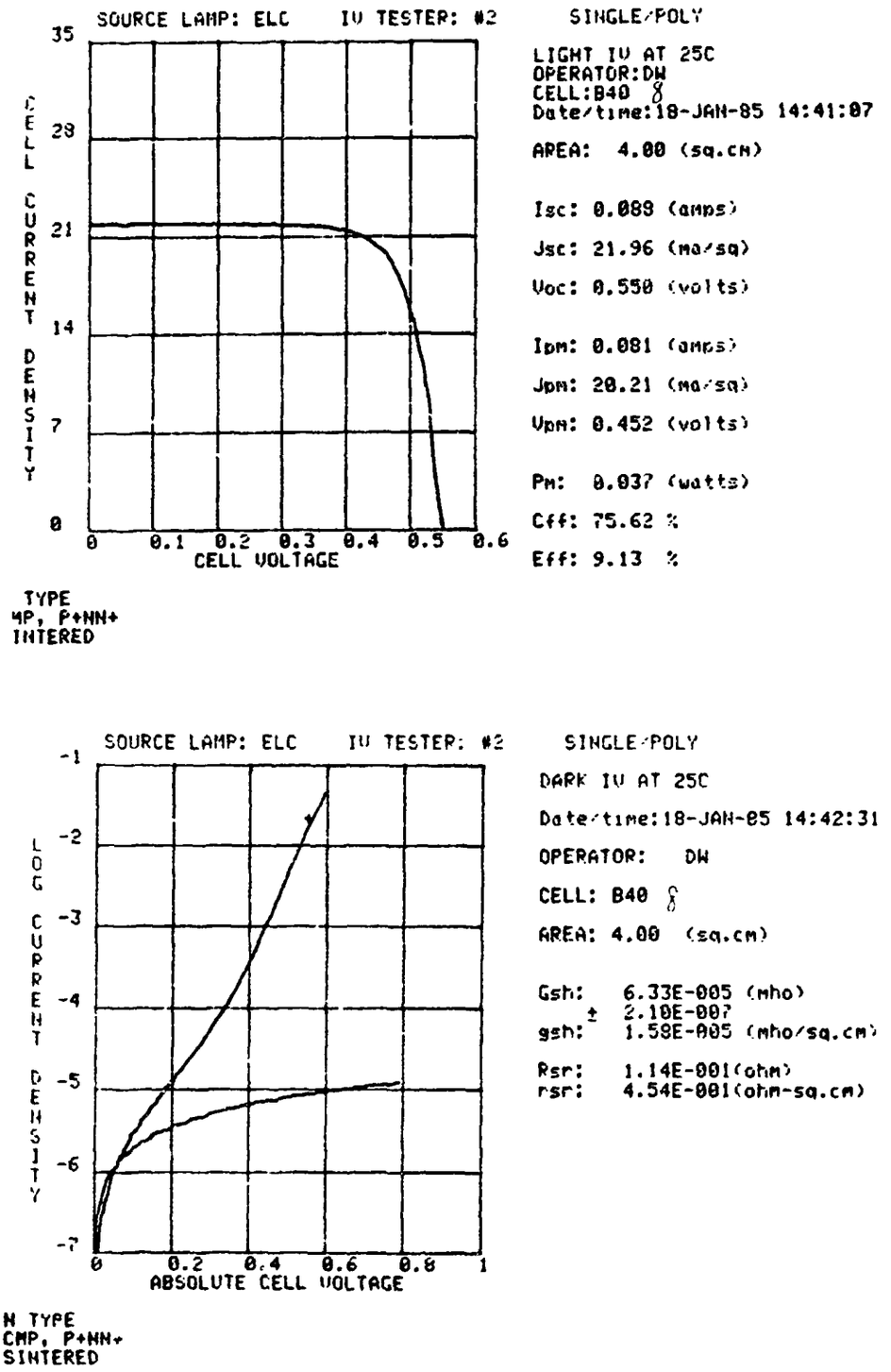


**Fig. 2-16.** Light and dark I-V curves of Batch 40 cells.

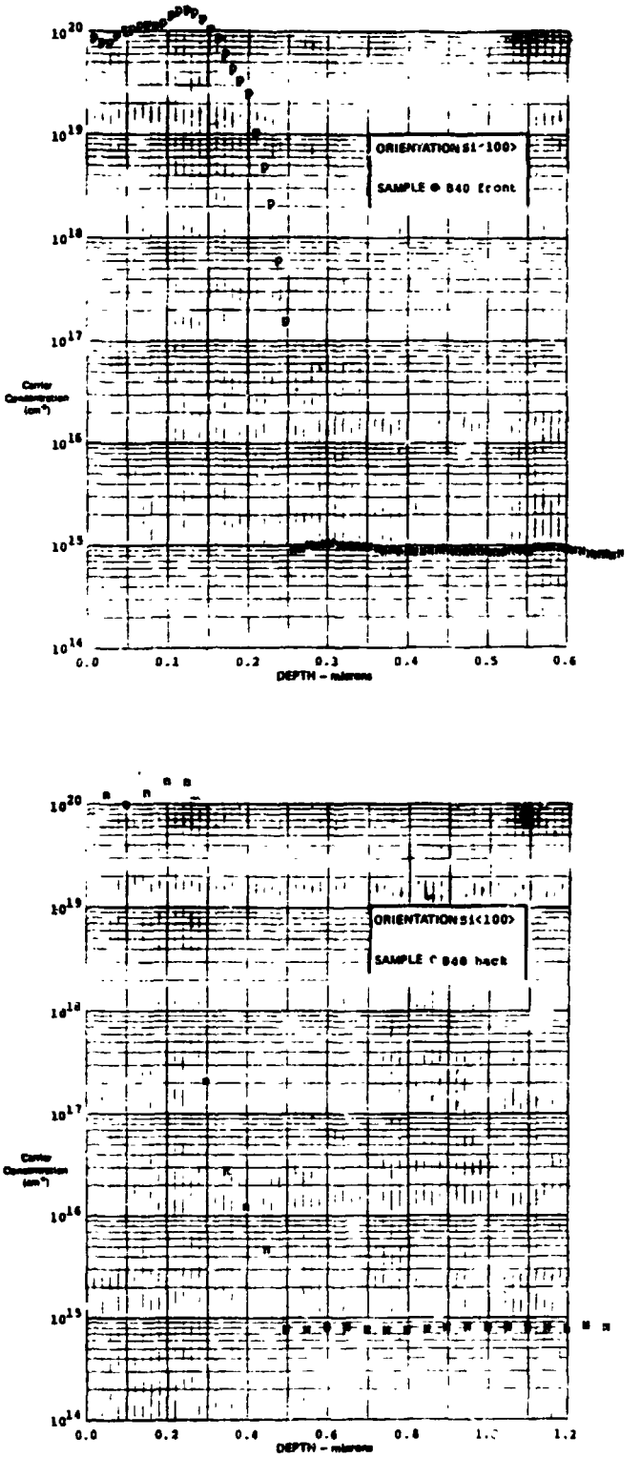


**Fig. 2-17.** Depth profiles of Batch 40 cells. Front junction boron. Ion implant energy 5 keV with fluence $3 \times 10^{15}$ atoms/cm$^2$, laser energy density at 1.4 J/cm$^2$, 50% overlap. BSF phosphorus ion implant at 15 keV, $1 \times 10^{16}$ atoms/cm$^2$, 50% overlap.

## SECTION 3.0
## DISCUSSION

While laser annealing is a true "cold" process that should not degrade bulk minority lifetime, it has many technical disadvantages in comparison with conventional thermal diffusion.

One disadvantage is that textured surfaces were not found suitable for the laser junction forming process due to difficulties in controlling the degree of surface melting. AR coatings must be employed in production for light absorption enhancement.

Another problem is that the process is extremely sensitive to surface conditions because the diffusion in laser annealing is carried out in the liquid state. Any scratches or defects on the surface are modified during the recrystallization. Surface defects/contamination increase the surface/bulk recombination rate which in turn decreases $V_{OC}$.

Ion implantation is a well-developed technology for integrated circuit processing and is especially useful for fabricating deeply buried junctions. However, in the fabrication of solar cells, the implanted layer must be shallow with sufficiently high surface concentration. In other words, solar cell junction formation requires low keV ($\lesssim$3 keV) with high ion fluence. 5 keV is the lowest available through commercial services or equipment. Even at such low kinetic energy implantation, deep lattice damage unremovable by 1.5 J/cm$^2$ laser energy density has been demonstrated in this phase of the project. Increasing the laser energy density for deeper melting might remove deep deposition damage defects, but heavy surface damage also takes place. Deep lattice damage can also be induced by neutralized implanting atoms during the conventional monoatomic ion implantation. These "neutrals" traveling with 35 keV kinetic energy are not decelerated by the reverse potential of 30 kV. Particles with such high impact energy are expected to penetrate deep into the substrate. Their effect on $V_{OC}$ can be realized by considering the following junction equation:

$$V_{OC} \cong \frac{kT}{e} \ln \frac{J_L}{J_{o1}+J_{o2}}$$

where

$J_L \sim J_{SC}$ = short circuit current density

$$J_{o1} \propto \sqrt{D/T}\ /N_A$$

$$J_{o2} \propto \frac{U}{N_B}$$

$N_B$ = bulk dopant concentration

$\frac{kT}{e} \approx 0.0254$ V at T = 300°K

U = recombination rate

An increase in U will obviously decrease the $V_{oc}$ as experimentally observed in ion implanted samples compared with non-ion implants. Technically, neutrals can be removed during implant. Experiments with newly prepared materials has begun.

Another vendor provided ion implant service by using a non-mass analyzed molecular beam. The dopant kinetic energy is proportional to the fraction of dopant atomic weight to the source ion molecular weight:

$$\text{dopant keV} = \frac{\text{dopant atomic wt}}{\text{molecular wt}} \times \text{electrode potential}$$

e.g.,

$$\text{boron atom energy} = \frac{\text{boron atomic wt}}{BF_2 \text{ molecular wt}} \times \text{beam energy}$$

$$= \frac{11}{49} \times 22 \text{ keV} \sim 5 \text{ keV}$$

This analysis is true only if the $BF_2$ molecule dissociates into atoms at the surface. Otherwise, the impact energy would be 22 keV, the effects of which are not certain at this time. The first experimental result obtained on an n-type substrate using molecular ion implantation yielded cells about 9% efficient, with BSF. It was decided to halt use of n-type substrates in this project due to complicated processing requirements. Molecular ion implant on the other hand could be promising for phosphorus implants due to the heavier atomic weight of phosphorus. The detrimental effect of the nondissociated molecule would not be as much as in $BF_2$ because of higher atomic mass, for example. The first attempt on p-type Cz wafers has yielded cell efficiencies above 9% without BSF. Better results could be obtained by fine tuning the new parameters such as beam energy and beam fluence.

# SECTION 4.0
# CONCLUSION

In general, the major technical barriers limiting the success of laser processing are the nonideal ion implant and wafer surface conditions, the effects of which are far more serious for laser annealing than conventional thermal diffusion processes.

## SECTION 5.0
## PROBLEMS AND PLANS

### 5.1 PROBLEMS

1. The lack of availability of uniform, low energy ion implant capability has seriously affected the ability to produce high efficiency laser processed cells. Commercially available sources all perform well when the implant energy is greater than 15 keV. Ion sources in the range of 1 to 5 keV are required.

2. The influence of surface condition before laser junction formation is much greater than previously assumed. Mechanical damage and surface cleanliness are both important. Much of the problem has been delineated but not completely solved.

3. The surface most likely to be used in a factory setting would be that resulting from a NaOH damage etch after sawing (called a Chemically Polished surface), rather than a Chem-Mechanical Polished surface. The work done in this study has been carried out on CMP surfaces in order to isolate important effects due to various surface conditions. There are still questions remaining about the performance of CP surfaces.

### 5.2 PLANS

1. Ship gas processing system to Spectra Technology and integrate with optical system.

2. Carry out laser-assisted CVD experiments for metallization and surface passivation of solar cells.

3. Complete processing of 25 2x2 cm high efficiency laser processed cells for delivery to JPL.

4. Initiate experiments on large area (93 cm square) Cz cells.

5. Continue investigation of junction improvement.

Program Tasks

I. Program Management

a. Subcontract Approval
b. Management

II. Process Selection

a. Target Process
b. Revision
c. Final Process Specification

III. Process Development

a. Annealing Study
b. Equipment Fabrication
c. Experimental Matrix
d. Deliver 25 2x2 cm cells

IV. Process Sensitivity Assessment

V. Process Verification

a. Cell Processing
b. Cell Characterization
c. Deliver 25 5.2" cells

VI. Laser Reliability and Appropriateness

VII. Cost Evaluation

VIII. Documentation

a. Program Plan
b. Laser Process Selection Report
c. Economic Analysis Report
   Preliminary
   Final
d. Monthly Progress Reports
e. Quarterly Progress Reports
f. Final Report
   Draft
   Final (one month after JPL comments)
g. Program Reviews as Required
h. PIM

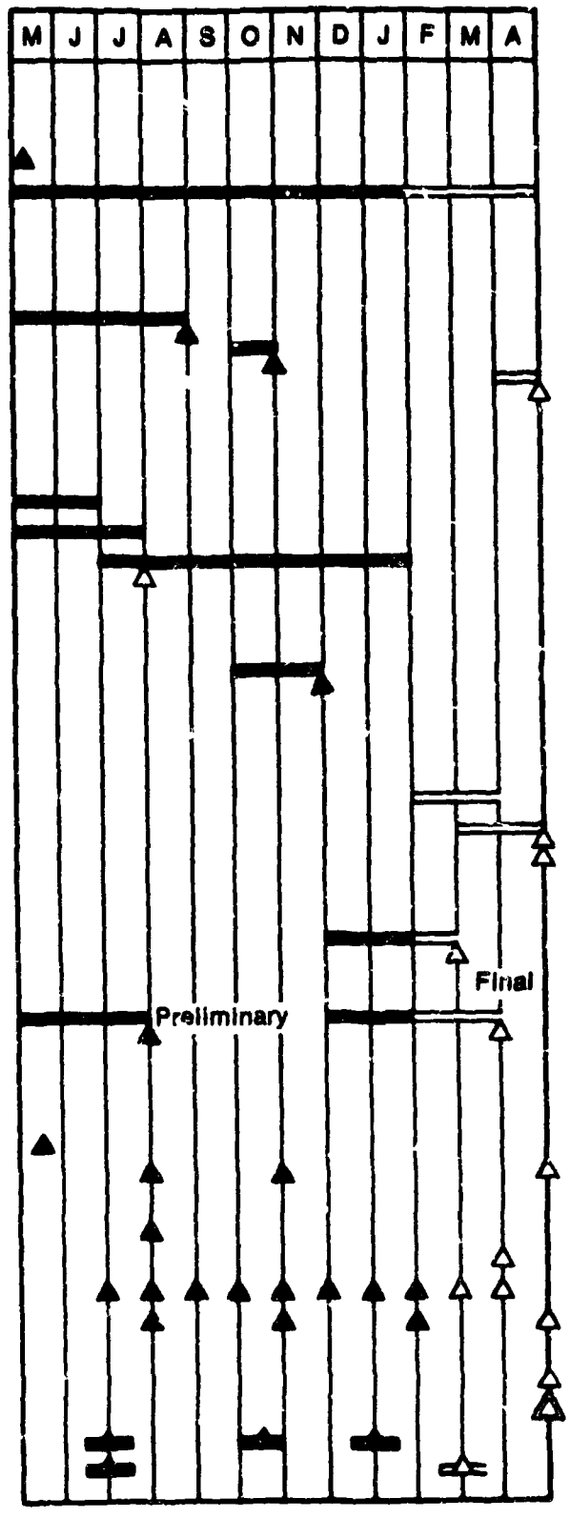


Fig. 5-1. Program schedule.

## REFERENCES

1. A. G. Cullis, D. T. J. Hurle, H. C. Webber, N. G. Chew, J. M. Poate, P. Baeri, and G. Foti. "Growth Interface Breakdown During Laser Recrystallization From the Melt." Appl. Phys. Lett. 38 (8), 642 (1981).

## ACKNOWLEDGMENTS

The authors would like to express their thanks for help received from Dorothy Houk, Mary McLaughlin, Mari Kristiansen, and Jim Wilson in preparing the report, and from Kim Blaker, Frank Unc, Liberty Elyash, Bill Ragland, and Bob Curtis in technical assistance. Continuous advice and encouragement given by Paul Alexander and Merle Larson are also highly appreciated.